Toward a more accurate Q value measurement of tritium: status of THe-Trap

**S. Streubel · T. Eronen · M. Höcker ·
J. Ketter · M. Schuh · R. S. Van Dyck Jr. ·
K. Blaum**

Abstract The goal of the THe-Trap experiment is to measure the tritium/helium-3 mass ratio in order to deduce the Q value of the tritium β-decay. A relative uncertainty of 10 parts per trillion in the mass ratio would allow determining the Q value with a precision of 30 meV. This value is of relevance for the Karlsruhe Tritium Neutrino (KATRIN) collaboration, which is building a spectrometer to measure the mass of the electron antineutrino. In this contribution, we present the progress made in the past 2 years. We can, e.g., store, manipulate and detect single ions. To demonstrate the current accuracy, we measured the carbon-12 to oxygen-16 mass ratio with a relative uncertainty of 120 parts per trillion in early 2013. The improvements, current status and future perspectives will be presented.

1 Introduction

In Penning trap mass spectrometry of nuclides with half-lives of more than 1 year, the tritium mass is perhaps the most challenging mass to measure. Whereas for all other nuclides, the mass-to-charge ratio can be pushed to a more favorable, lower number by charge breeding, the tritium atom has only one electron to be removed. Another issue is the radioactivity of tritium. Although its β-decay half-life

S. Streubel (✉) · T. Eronen · M. Höcker · J. Ketter ·
M. Schuh · K. Blaum
Max Planck Institute for Nuclear Physics, Saupfercheckweg 1,
69117 Heidelberg, Germany
e-mail: sebastian.streubel@mpi-hd.mpg.de

R. S. Van Dyck Jr.
Physics Department, University of Washington, Seattle,
WA 98195, USA

of 12.3 years is sufficiently long to use the same experimental techniques as for stable nuclei, the presence of tritium can easily disturb the measurement once it is adsorbed on the surfaces of the trap. The electrons emitted due to the β-decay of tritium can cause, for instance, spontaneous loading of the trap with contaminant ions [1].

The tritium β-decay Q value is defined as the atomic mass difference between tritium and helium-3. It is of particular interest for the KATRIN experiment [2], which is currently under construction. The KATRIN collaboration aims to investigate the mass of the electron antineutrino by measuring the energy spectrum of electrons emitted in the tritium β-decay. Near the endpoint, the shape of the spectrum is sensitive to a non-zero neutrino mass.

KATRIN is designed to either measure the neutrino mass with a precision of 0.3 eV/c^2 or alternatively give an upper limit of 0.2 eV/c^2 with 95 % C. L. These values are approximately a factor of ten smaller than the 95 % C. L. upper limits of 2.12 and 2.30 eV/c^2 that the two precursor experiments "Troitsk ν-mass" and "Neutrino Mainz" determined, respectively [3, 4]. It is worth noting that the neutrino mass determination by these spectrometers is based on kinematics, with only minor theoretical corrections needed to correct for the final ^{3}HeT$^+$ molecular ion excitation energy [5].

The observation of neutrino oscillations has indicated that at least two of the three neutrino flavors have a non-zero mass. Stellar observations, in combination with cosmological models, impose an upper limit on the sum of the neutrino masses. The most stringent ones are 0.28 eV/c^2 [6] and 0.29 eV/c^2 [7], both with 95 % C. L. The exact value of the limit depends heavily on the underlying theoretical models. A third indication of the finite neutrino mass could come from the observation of neutrinoless double-beta decay. One controversial report claims to have

observed such decays and calculated a neutrino mass of $(0.2–0.6)$ eV/c^2 [8]; the second-generation experiment GERDA, however, could not reproduce the observation [9]. Penning trap mass spectrometry has contributed to these types of studies with numerous Q value measurements for locating the endpoints of the beta spectra [10]. In all three fields, there are ongoing experiments.

The experimental setup THe-Trap will contribute to the neutrino mass studies by measuring the position of the endpoint of the tritium β-decay spectrum with an uncertainty of 30 meV, requiring a relative uncertainty of 10^{-11} of the parent-to-daughter mass ratio itself. As discussed in Refs. [5, 11], the measurement provides an important systematic check for the KATRIN data. The KATRIN experiment is a special type of retardation spectrometer. The precise value of the endpoint it measures relies on the calibration of an 18.6 kV voltage source and is influenced by subtle details such as surface charges and the work function of the materials used for the electrodes and the tritium source. The effective retardation potential of KATRIN has to be stable on a 60-mV level during measurement runs that typically last 2 months [12]. In practice, the Penning trap Q value cannot be used to constrain the fit to the KATRIN data. To be useful, this would require both the Penning trap Q value and the absolute energy calibration of KATRIN to be measured at the meV level.

The most precise atomic mass ratios have been measured with Penning traps utilizing non-destructive detection methods of the stored ion and reached relative uncertainties on the level of 10^{-11} [1, 13, 14]. However, this kind of precision has only been reached for stable

isotopes or molecules; difficulties encountered with radioactive tritium are described for instance in Ref. [1]. The evolution of the uncertainty in the tritium Q value over the years is illustrated in Fig. 1. The most recent value by Nagy et al. [15] was measured with a Penning trap method that is somewhat limited in precision but ideal for short-lived radioactive ion species [16, 17]. This experiment reached a relative uncertainty of 4×10^{-10} in the mass ratio, which corresponds to a precision of 1.2 eV in the Q value.

In the following sections, we will describe the details of the THe-Trap experiment, including how to minimize the tritium contamination and efforts needed for achieving the desired precision. We also show results of our recent ^{12}C^{4+} to ^{16}O^{5+} mass ratio measurement that demonstrates the current precision.

2 Experimental setup

THe-Trap was built and designed at the University of Washington, Seattle, USA [1]. After construction [22] and preliminary tests [23], the setup was shipped to the Max Planck Institute for Nuclear Physics, Heidelberg, Germany, in 2008. The recommissioning and principal functionality of the experiment was described in a previous publication [24]. Since then, the setup was renamed from MPIK/UW-PTMS to THe-Trap, which stands for *T*ritium–*He*lium-3-*Trap*, in order to better reflect the purpose it has now been dedicated to. Since there have been no major hardware changes affecting the general layout of the setup, we only give a short overview here.

2.1 Trap design

The central part of the experiment is an electrode stack that forms two hyperbolical Penning traps: the upper trap and the lower trap. These will allow us to trap two ions simultaneously, storing one ion in the upper trap while measuring the frequencies of the other ion in the lower trap. A cyclotron frequency ratio measurement will be performed by periodically exchanging the position of the ions. Figure 2 shows a cross section of the lower trap, which is the one used for the measurements reported here. The upper trap is identical with the exception of larger hole sizes for the endcaps and skimmers.

The ability to store both ions and to exchange them within minutes allows not only a speedier measurement cycle (1 h vs. 3 days per ion pair [25]) but also removes the need to constantly reload the trap, thus minimizing contamination of the trap electrodes with radioactive tritium. Compared to the coupled magnetron orbits technique [13] 1 h of measurement time is still long, but our measurement
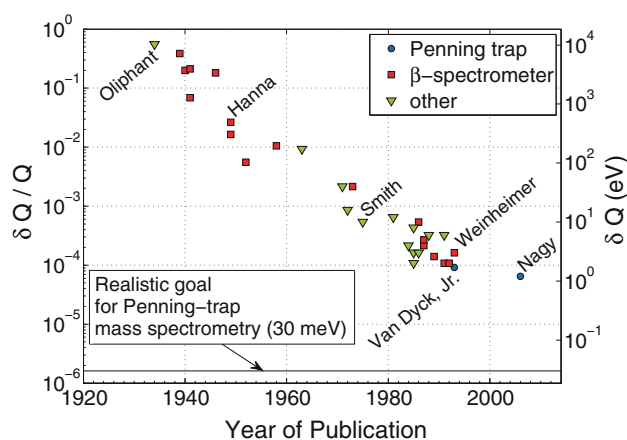

Fig. 1 Since the discovery of tritium in 1934 by Oliphant et al. [18], its decay energy has been determined with several different techniques. These include, among others, rather accurate β-endpoint spectrometers, e.g., by Hanna et al. [19] and radio-frequency (RF) spectrometers starting with Smith et al. [20]. The last value by a β-endpoint spectrometer was measured by "Neutrino Mainz" [4], one of the predecessor experiments of KATRIN. The most recent values are measured by Penning trap mass spectrometers [15, 21]
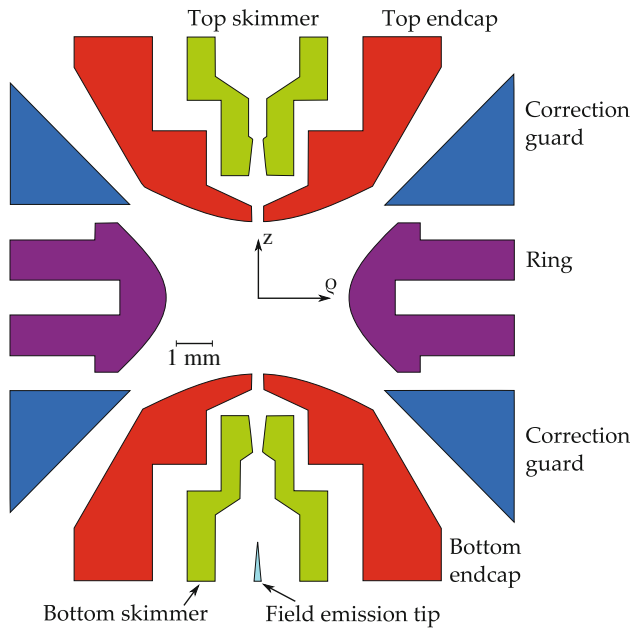
Fig. 2 A cross section of the lower Penning trap used for the measurements reported here. The endcaps are used for detection and kept at (dc) ground potential, while the quadrupole trapping field is applied with ring and guard electrodes. The guards are azimuthally twofold split and also used to apply RF drives. The field emission tip is used to create a beam of electrons that can be used for ion loading

method will not be limited by ion–ion interaction effects. For the time being, ion transport and external ion loading are yet to be implemented.

2.2 Measurement principle

Penning trap mass spectrometry is based on the fact that a charged particle moving perpendicular to a magnetic field B_0 is forced onto a circular orbit with the so-called free-space cyclotron frequency

$$v_c = \frac{\omega_c}{2\pi} = \frac{1}{2\pi}\frac{q}{m}B_0, \tag{1}$$

where q and m are the particle's charge and mass, respectively. In addition to the trap's magnetic field, which confines the radial motion of the charged particle, a coaxial electrostatic quadrupole potential is applied to confine the axial motion. This is called a Penning trap. The additional electrostatic potential causes the cyclotron motion to split into two trap-specific radial motions: the magnetron motion and the *modified* cyclotron motion. In the presence of ideal fields (i.e., perfectly homogeneous magnetic field and quadrupole electrostatic potential) with perfect alignment, the frequencies of the three trap-specific motions are

$$v_z = \frac{1}{2\pi}\sqrt{\frac{qV_0}{md^2}}, \tag{2}$$

$$v_\pm = \frac{1}{2}\left[v_c \pm \sqrt{v_c^2 - 2v_z^2}\right], \tag{3}$$

where v_z, v_- and v_+ are the frequencies of the axial, magnetron and modified cyclotron motions, respectively. $V_0 = V_{endcap} - V_{ring}$ is the voltage applied across the ring and the endcap electrodes (at THe-Trap, the endcaps are kept at ground potential, and thus, a negative V_{ring} is needed for positively charged ions) and d the characteristic trap size (design value of THe-Trap $d = 2.12$ mm at room temperature). From these frequencies, the free-space cyclotron frequency can be determined through the invariance theorem [26]

$$v_c^2 = v_z^2 + v_-^2 + v_+^2, \tag{4}$$

which holds true for traps with a non-zero ellipticity and misalignment of the electrostatic field. When the free-space cyclotron frequency v_c is determined for two ions in the same magnetic field B_0, one can calculate their mass ratio m_1/m_2 by taking the inverse of the free-space cyclotron frequency ratio and correcting for possibly different charge states, missing electrons and their binding energies.

At THe-Trap, only the axial motion is observed directly with a high-quality-factor tuned circuit connected across the endcap electrodes. The axial motion is excited with a constant radio frequency (RF) drive at a frequency close to the resonance of the detection circuit (approximately 4 MHz). The ion's response is amplified and mixed with the original drive signal in order to generate a DC error signal. By choosing appropriate phase shifts at the mixer input, a dispersion-shaped signal is created and deviations of v_z from the drive frequency are observed either as negative voltage or as positive voltage, depending on the sign of the difference. By integrating the error signal and adding it to the ring voltage, the axial frequency can be kept constant. Thus, any change that causes the natural axial frequency to shift is compensated for by a change in the ring voltage. This is called an *axial frequency lock*. With a maximum ring voltage of -100 V, ions with an m/q up to ≈ 3.25 u/e can be used for measurements.

The radial frequencies are determined by exploiting anharmonicities of the trap. For a cyclotron energy E_+, the relative axial frequency shift is

$$\frac{\Delta v_z}{v_z} = \left[\frac{B_2}{B_0 m\omega_z^2} - \frac{1}{2mc^2} - \frac{3C_4}{qV_0}\left(\frac{v_z}{v_+}\right)^2\right]E_+, \tag{5}$$

where the three lowest-order contributions are listed inside the square brackets. The first term is caused by the magnetic bottle effect (factor B_2 describes its magnitude), the second is due to the relativistic mass increase, and the third

is due to an electrostatic anharmonicity (term C_4). The radial frequencies are determined by sweeping the frequency of an RF drive (applied to one of the split guards) a few 10's of mHz around the expected frequency. When the sweep matches one of the radial frequencies, energy is transferred into the addressed motion and the axial frequency starts to shift. As the axial frequency is locked, the ring correction voltage changes to counteract the shift, thereby revealing the radial frequency. The anharmonicities also cause the radial frequencies to shift during this type of measurement. To interpolate to the frequency of the undisturbed motion, two sweeps are performed in opposite directions.

Instead of measuring the magnetron frequency ν_- directly, the magnetron-to-axial coupling frequency $\nu_- + \nu_z$ is determined. Although this introduces some additional uncertainty, its contribution to the final free-space cyclotron frequency ν_c is small as seen from maximum error propagation on Eq. (4)

$$\frac{\delta\nu_c}{\nu_c} = \left(\frac{\nu_+}{\nu_c}\right)^2\left|\frac{\delta\nu_+}{\nu_+}\right| + \left(\frac{\nu_z}{\nu_c}\right)^2\left|\frac{\delta\nu_z}{\nu_z}\right| + \left(\frac{\nu_-}{\nu_c}\right)^2\left|\frac{\delta\nu_-}{\nu_-}\right|, \qquad (6)$$

in which the relative frequency uncertainties $\delta\nu_i/\nu_i$ are scaled by the ratios $(\nu_i/\nu_c)^2$. To reach a precision of $\frac{\delta\nu_c}{\nu_c} = 10^{-11}$ with typical ion frequencies ν_+, ν_- and ν_z of about 26, 0.3 and 4 MHz, they need to be determined better than 0.3, 30 and 2 mHz, respectively. The requirement for the magnetron frequency precision is very modest, and a precision of $\delta\nu_- < 20$ mHz is routinely obtained. We observed that the magnetron frequency is stable on this level over months.

2.3 Ring voltage supply

The stability requirements for the ring electrode voltage supply are demanding. Nominally, a stability of better than 10^{-7} for a voltage of 100 V on a timescale of 10 min is required to distinguish axial locked-loop action from voltage drifts. Also, the short timescale jitter of the voltage needs to be small enough to keep the axial frequency jitter below the axial linewidth. The currently used voltage source is a prototype device developed for the PENTATRAP experiment [27, 28] at the Max Planck Institute for Nuclear Physics in Heidelberg. The previously used voltage source described in Ref. [29] only had a computer-controlled output range of -90 to -80 V. The new voltage source allows computer control over the full -100 to 0 V output range with 1-μV resolution and similar stability. The relative voltage fluctuations on the relevant timescale between 1 and 1,000 s are about 3×10^{-8}, which is stable enough to perform frequency measurements. A more comprehensive description of the voltage source will be given in Ref. [30].

2.4 Controlling the environmental parameters

An important step in high-precision Penning trap mass spectrometry is to keep the magnetic field as stable as possible. The fluctuations during the measurement period must not be greater than the aimed frequency precision, since the frequency is directly proportional to the magnetic field. The biggest field fluctuations originate from the materials used for the cryostat of the superconducting magnet due to temperature-dependent susceptibilities.

Great care has been taken to counteract these effects. The original stabilization system from the University of Washington [31] has been reassembled in Heidelberg with some additions. In the following, the relevant parts of the stabilization system are described.

Helium gas pressure above the liquid helium This pressure is stabilized to 0.01 Pa against a temperature-controlled absolute pressure reference volume at about 1,040 hPa. This reference varies by about 0.5 Pa due to temperature changes in the surrounding room. This corresponds to a relative cyclotron frequency variation of 8 ppt.
Liquid helium level in the magnet bore This level is stabilized to approximately 10 μm, which corresponds to a 3.5-ppt variation in the cyclotron frequency.
Use of a self-shielding superconducting magnet The magnet used in the experiment is a self-shielding type [32] with a suppression factor of up to 180 for external field fluctuations at the position of the lower trap. A typical daily variation of 100 nT of the external magnetic field leads to a remaining variation of about 100 ppt of the 5.27 T trap field.
A coil pair in Helmholtz configuration for eliminating external field fluctuations Combined with a custom-built fluxgate magnetometer, the coils actively cancel external fluctuations with another factor of at least 10, reducing the daily variations below the 10 ppt level.
Vibration damped ground The floor that the magnet rests on is isolated from the rest of the building. Vibrations are damped to better than 1 μm/s at 50 Hz.
Temperature stabilized room The stabilization to 24.5 °C is arranged by controlling the electrical heating of the room. The major part of the heat flows through a wooden wall to a neighboring room, which is kept about 6 °C colder. This way the temperature fluctuations stay below 30 mK at the reference temperature measurement point of the system. The source–sink arrangement leads to temperature gradients in the room, which are also affected by ambient conditions. A temperature sensor near the wooden wall shows a typical variation of less than 150 mK on a timescale of several days.
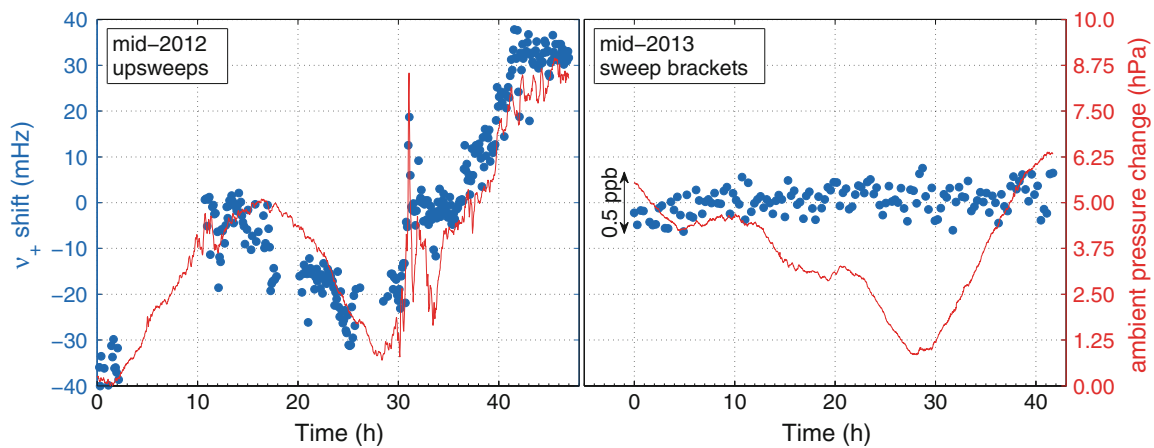
Fig. 3 Temporal fluctuation of the magnetic field measured by repeatedly recording the modified cyclotron frequency of a $^{12}C^{4+}$ ion (shown as *blue solid circles*, *left axis*) and concurrent changes in the ambient pressure (*red line*, *right axis*). *Left* In mid-2012, the modified cyclotron frequency was strongly pressure dependent. Also, at that time, C_4 was not tuned properly and only the upsweeps produced valuable data. *Right* More recent measurements from mid-2013 show a lower dependency. Between the two datasets, improvements to the mechanical coupling of the trap structure and the magnet were made

The measured stability of the cyclotron frequency is plotted in Fig. 3. We assume that changes in the ambient pressure shift the position of the superconducting magnet coils relative to the cryostat and the traps. Since the magnetic field is inhomogeneous (due to the cryostat materials, improper shimming and a buildup of air ice inside the magnet bore), the position shift causes a free-space cyclotron frequency change.

Also, one of the two liquid helium filling ports was blocked by frozen air. In the design of the magnet, the magnet coils and the Penning traps have the same mounting point, and thus, any external movement keeps the relative position of the coils and the traps constant. The frozen air could have caused a second fixed point between the magnet and the traps, thereby increasing their relative movement. The ice could not be removed during the measurement campaign because of a high risk of quenching the magnet. We could, however, reduce the pressure dependency by increasing the mechanical coupling at the designed point, see right figure in Fig. 3. On a timescale of days, we can observe a relative field drift of a few ppt/h. For reasons that are under investigation, the drift is occasionally worse and can exceed a few 10 ppt/h.

3 Current progress

The previous progress with THe-Trap in Heidelberg was reported in Ref. [24]. By then, the system had been commissioned and some initial ion work could be reported such as measurement of all eigenfrequencies with clouds of ions. Now, we routinely work with single ions.

3.1 Ion loading and patch potentials

A typical loading procedure using the electron field emission point below the lower trap causes the trap to be filled with several ion species. The usual way to remove the contaminants is to excite their axial motion to large amplitudes while cooling the ion of interest. A subsequent reduction in the ring potential to some few -10's of mV expels the hot contaminants from the trap. Part of the electron beam used for trap loading hits the endcap electrodes causing negative charges to accumulate on the surfaces of the electrodes, which shift the center and anharmonicity of the trap. When ion loading is needed between the measurements of different ion species, this causes the frequency shifts to be different from measurement to measurement.

To see whether the loading procedure was successful and created only a single ion, one can observe the lock voltage and the modified cyclotron frequency over time as any remaining contaminant ions will change both quantities significantly. Furthermore, the number of ions of the species of interest can also be measured directly. The measured width of the driven axial resonance [33] is directly proportional to the number of ions of the species being driven. Other species affect the linewidth in a more subtle way. In Fig. 4, a typical resonance for a single $^{12}C^{4+}$ ion is shown. The phase between the detection and the drive is chosen such that the curve has a dispersion-shaped profile, and thus, the detected DC error signal is zero at the natural resonance frequency.
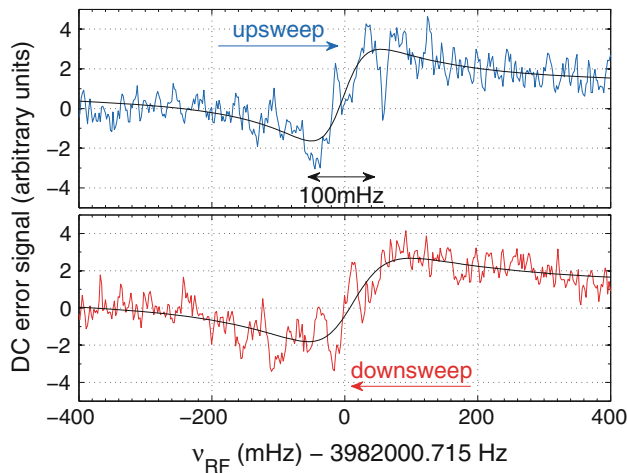
Fig. 4 An RF drive sweep over the natural axial frequency while keeping the ring voltage constant. The detected resonance is tuned to be of dispersion shape. The width of the resonance is proportional to the number of ions. and the detected signal is proportional to the RF drive strength. Here, the resonance width of 100 mHz obtained from the fit (*solid lines*) indicates a single $^{12}C^{4+}$ ion. For the measurement of ν_+, we tune the ring voltage so that the natural axial frequency will match the detection frequency of 3,982,000 Hz
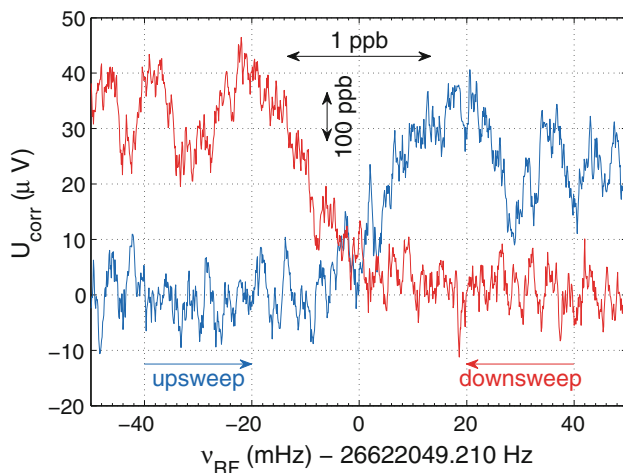

Fig. 5 Two RF drive sweeps over the modified cyclotron frequency ν_+. When energy is transferred to the ion, the natural axial frequency changes, and hence, the axial locked-loop has to correct the ring voltage of about -87.6 V by U_{corr} to keep the axial frequency constant. After each sweep, the cyclotron energy is removed with radial cooling. By introducing a small C_4 (by changing the voltage of the correction guard electrodes), one can tune the sweeps to be symmetric. The final value 26,622,049.210(4) Hz for ν_+ is obtained from the intersection of the two sweeps

3.2 Determination of the modified cyclotron frequency

As described in Sect. 2.2, the modified cyclotron frequency is measured by sweeping an RF drive over the ν_+ frequency and observing changes in the voltage that the axial locked-loop has to apply to the ring electrode in order to

keep the axial frequency constant. This procedure has been improved significantly since the publication of Ref. [34]. With single-ion detection, the voltage range of the locked-loop could be decreased and the frequency sweeps could be done with a much narrower range, see Fig. 5. With a nominal sweep range of 100 mHz and duration of 200 s, a resolution of about 3 mHz can be obtained for a sweep bracket consisting of a frequency up- and downsweep. Ultimately, the resolution is limited by the sweep duration and range. For tritium or $^{12}C^{4+}$ ions having a modified cyclotron frequency of about 26 MHz, this corresponds to a resolution of 1×10^{-10}.

Also like the axial frequency, the radial frequencies shift when the ion gains energy in the radial modes. For the modified cyclotron motion, the relative shift, in first order, is given by

$$\left.\frac{\Delta\nu_+}{\nu_+}\right|_{lock} = \left[-\frac{1}{mc^2} - \frac{3C_4}{2qV_0}\left(\frac{v_z}{v_+}\right)^4\right]E_+, \quad (7)$$

where the first term inside the square brackets is due to relativistic mass increase and the second term due to electric field anharmonicity through the C_4 term. Without axial frequency lock, there would also be a contribution from the B_2 term [35]. In a well-tuned trap (i.e., $C_4 \approx 0$), the relativistic shift causes the modified cyclotron frequency to decrease as cyclotron energy is increased. This means that while performing downsweeps, the resonance frequency follows the drive, and thus, more energy is added to the motion. This is referred to as *frequency pulling*. The effect is opposite in upsweeps, and thus, even less energy is added to the motion. The early attempts focused on making the axial mode harmonic, i.e., setting $C_4 \approx 0$. Later, it was found that this not only made the cyclotron mode anharmonic with respect to the cyclotron energy E_+ but also the axial shift with respect to cyclotron energy was less pronounced, and consequently, stronger cyclotron drives were needed.

To minimize pulling on either sweep direction, the relativistic mass shift term in Eq. (7) was compensated with an appropriate C_4 setting (see Fig. 5). The drawback is that the non-zero C_4 causes the radial frequencies to depend on the axial energy that is used for detection. Ideally, this energy can be slightly lower than the thermal limit given by the 4 K detection circuit, but for the time being, the needed energy is several times bigger. The reasons for why such high amplitudes are needed are under investigation. For mass doublets like $^3H^+/^3He^+$, these shifts vanish to a large extent, but for non-doublets, they need to be corrected for.

To quantify them, the modified cyclotron and magnetron frequencies have been recorded with different axial drive strengths, see Fig. 6. In order to correct for the shifts, the curves are extrapolated to zero-strength drive. For a pure
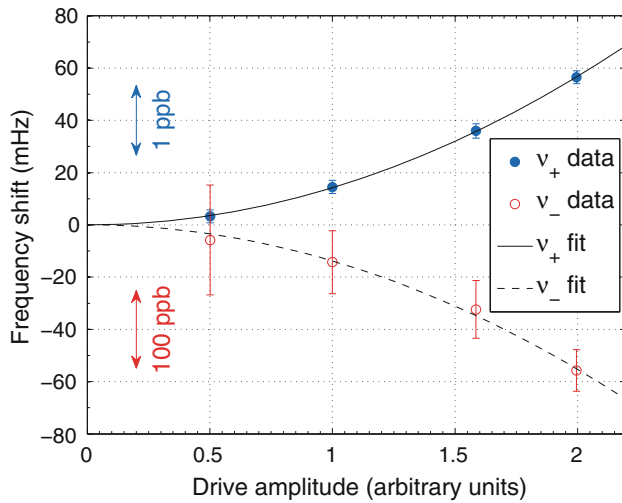
Fig. 6 Frequency shifts of the modified cyclotron and magnetron frequencies as a function of the axial drive strength due to anharmonicities. The data clearly have the expected quadratic dependency on the amplitude as shown by the fits (*lines*). The *vertical axis* offset is chosen to match the limit of no drive strength. With a typical drive strength of "1", we have a correction of about 14 mHz in both of these frequencies

Table 1 Simulated coefficients of the electrostatic potential generated by the ring electrode (C_n' coefficients) and guard electrodes (D_n coefficients) for the two traps

n	C_n'	D_n
Upper trap		
2	-0.98	-2.11×10^{-3}
4	1.72×10^{-2}	-2.14×10^{-2}
6	3.81×10^{-3}	4.82×10^{-3}
Lower trap		
2	-0.99	-2.24×10^{-3}
4	1.17×10^{-2}	-2.16×10^{-2}
6	-2.17×10^{-3}	4.65×10^{-3}

The traps only differ by the hole radius in the endcap electrodes, needed for transporting ions and for the electron beam from the field emission point. The design radii of the holes are 152.5 and 371 μm for the lower and upper traps, respectively. Simulation uncertainties of the values are well below the given numerical precision

C_4 contribution, when the modified cyclotron frequency increases with stronger drive strengths, the magnetron frequency decreases by the same amount. Thus, the shifts mostly vanish for the sideband frequency $\nu_+ + \nu_-$ [36], which sums up to the free-space cyclotron frequency ν_c, assuming negligible energy in the radial modes. The uncertainty of the magnetron data can be further improved with more statistics, but since the magnetron frequency is only needed with modest precision, this is not necessary.

3.3 Electrostatic properties

As shown in Eqs. (5) and (7), the anharmonicities of the electrostatic potential shift the frequencies of the ion motion. To understand the electrostatic properties of THe-Trap, extensive simulations have been conducted with "COMSOL Multiphysics 4.2a" including the "AC/DC Module." The main motivation was to extract the coefficients of the polynomial expansion of the trap potential. For simulations, the trap electrodes are implemented using two symmetries, which greatly speed up the calculations: cylindrical symmetry and mirror symmetry about the plane going through the middle of the ring electrode. The reliability of the software is tested by varying the resolution of the simulation and also with other consistency checks.

For fitting the simulated electrostatic potential, the function

$$\Phi(r, \theta) \approx \frac{V_0}{2} \sum_{n \, \text{even}} A_n \left(\frac{r}{d}\right)^n P_n(\cos(\theta)) \tag{8}$$

is used. The summation is only performed over even coefficients since the contribution from odd terms vanishes due to reflection symmetry. The polynomial coefficients A_n are deduced for the ring electrode (denoted C_n') and for the guard correction electrodes (denoted D_n), while P_n are the Legendre polynomials. The effective C_n is the combined influence from C_n' and D_n. The simulations also take the shrinking of the trap when cooling from room temperature to 4 K into account. The fitting was conducted up to order $n = 10$, and the coefficients up to order 6 are given in Table 1. Further investigations have shown cubic dependencies of the coefficients on the hole radius in the endcap as in Ref. [35]. The simulated values match the experimentally deduced coefficients rather well. For example, the needed guard voltages to make the trap axially harmonic calculated from simulations and measurement deviate only by 4 %. Further improvements will require a better knowledge of the thermal expansion coefficients, patch potentials and actual dimensions of the trap geometry, which might differ from the design due to, e.g., gold plating and machining tolerances.

3.4 $^{12}\text{C}^{4+}/^{16}\text{O}^{5+}$ mass ratio measurement

To quantify the current performance of our experiment, a $^{12}\text{C}^{4+}$ to $^{16}\text{O}^{5+}$ mass ratio measurement with single ions was performed. Both masses are already well known and are thus well suited for a test measurement: Carbon is the atomic mass standard, and the mass of ^{16}O is known to about 1×10^{-11} relative uncertainty [1]. Although both carbon and oxygen ions can be created with the field emission point, oxygen was problematic due its low abundance in our trap. To overcome this issue, a larger

electron current from the field emission point was used, but this caused two unwanted side effects. First, as already explained earlier, one of the endcaps became slightly more charged up in every loading procedure. Second, more gas was released from the electrode surfaces, which in part spoiled the vacuum, reducing the typical ion lifetime. In the final setup with external ion creation and the possibility to transfer ions from the ion source to the traps as well as between the two traps, the charging will not be an issue.

The axial (and also detection) frequency was locked to 3,982 kHz in order to coincide with the resonance frequency of the tuned circuit. Provided that a single ion of interest is in the trap, the scheme to measure the radial frequencies is to

1. Cool the magnetron and cyclotron motion (4 min)
2. Establish the axial frequency lock (1 min)
3. Sweep the RF drive over the resonance frequency (3–10 min).

This scheme is repeated until enough statistics have been accumulated by the alternating upsweeps and downsweeps. Since the magnetron frequency does not need to be determined with a very high precision, it is measured only for a short time before and after the modified cyclotron frequency measurement.

The modified cyclotron frequency measurement procedure is illustrated in Fig. 7. The two ion species of interest denoted A and B correspond to $^{12}C^{4+}$ and $^{16}O^{5+}$ ions, respectively. First, a sufficient amount of consecutive upsweeps and downsweeps (usually 4 each) are performed with species A to obtain the average modified cyclotron frequency $\bar{\nu}_{+,A1}$ (top left box). Then, the trap is reloaded with ion species B, for which the same measurement procedure is applied (the box below), and then, species A is loaded again and so on. The ν_+ and ν_- frequencies are corrected for axial drive-dependent shifts. Also, these frequencies are corrected for the image charge shifts by 2.51 mHz per charge as described in Ref. [1]. Due to a
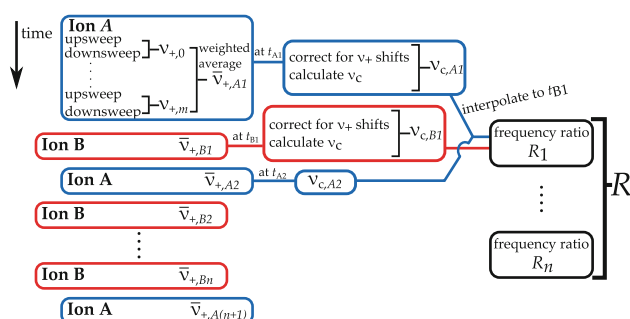

Fig. 7 The scheme for measuring the reduced cyclotron frequencies ν_+ and determining the free-space cyclotron frequency ratio R of ion species A and B (here $^{12}C^{4+}$ and $^{16}O^{5+}$, respectively). See text for more details

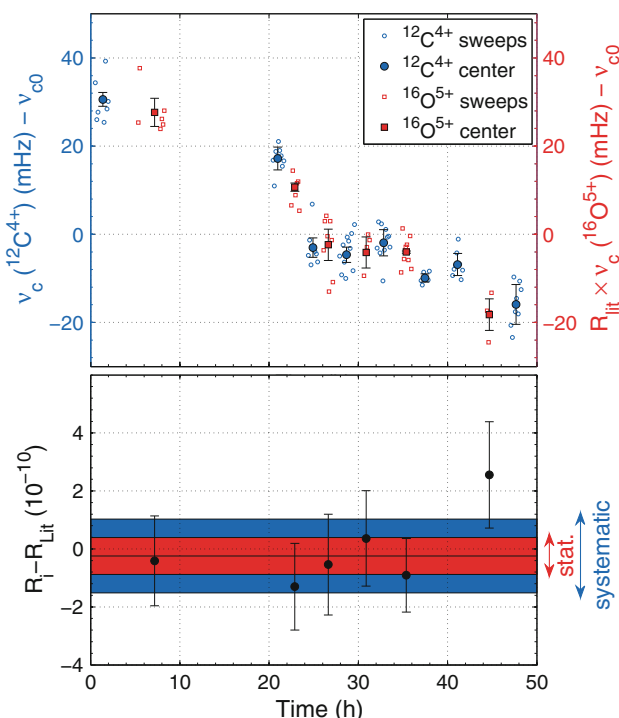**Fig. 8** *Top* Individual measurements of the cyclotron frequencies for $^{12}C^{4+}$ and $^{16}O^{5+}$ ions. The data show a magnetic field drift of about -38 ppt/h during the measurement period. The *small open symbols* indicate individual sweep centers and big filled symbols their average. An offset frequency of $\nu_{c0} = 26{,}919{,}853.520$ Hz is subtracted. *Bottom* The calculated cyclotron frequency (ν_c) ratios R_i from the data shown on *top*. The *smaller horizontal band* shows the final statistical uncertainty and the *larger band* the systematic uncertainties. The literature value deviates only by 24 ppt from the measured value

Table 2 Results of the $\nu_c\left(^{12}C^{4+}\right)/\nu_c\left(^{16}O^{5+}\right)$ measurements

Statistical uncertainty	63 ppt
$^{12}C^{4+}$ systematic	10 ppt
$^{16}O^{5+}$ systematic	120 ppt
Total systematic	120 ppt
Frequency ratio (measured)	1.066 339 779 162(63)$_{stat}$(120)$_{syst}$
Frequency ratio (literature)	1.066 339 779 186(12)
Difference	0.000 000 000 024

The binding energies of the atomic electrons are from Ref. [37] and the literature frequency ratio is calculated based on values from Ref. [1]

smaller magnetic field, the original value of 2.23 mHz per charge given in that article had to be scaled. The free-space cyclotron frequencies ν_c are calculated for both ions. A frequency ratio for each measurement of B is calculated by linearly interpolating the cyclotron frequency of A to the time of each measurement B. The final cyclotron frequency ratio R is obtained from the weighted average of the individual ratios.

By collecting data in a period of 2 days, a statistical uncertainty of 63 ppt was reached for the cyclotron frequency ratio. The axial drive-dependent systematic shift (see Fig. 6) was measured for $^{12}C^{4+}$ ions with an uncertainty of 10 ppt relative to the cyclotron frequency. Due to poor vacuum conditions in the trap volume, it was not possible to measure these shifts for the $^{16}O^{5+}$ ion, but a similar uncertainty can be attained with better conditions. This gives a lower boundary on the systematic uncertainty that we can currently reach. Using estimates for the C_4 and the axial amplitude that were used for the $^{16}O^{5+}$ measurement, we can correct for the shift to its cyclotron frequency with an uncertainty of 120 ppt. All the collected data are shown in Fig. 8, and the final results are summarized in Table 2. As can be seen, the literature value [1] is reproduced well within the statistical uncertainty.

4 Conclusion and outlook

Significant progress has been made since the last status publication in 2011 [24]. Since then, both traps have been used with single ions of different ion species as a matter of routine. Statistical uncertainties have been pushed down, reaching now routinely the sub-10^{-10} level. The leading systematic uncertainty stems from axial amplitude-dependent frequency shifts, which can be currently corrected at the 1.4×10^{-11} level.

A few hurdles still remain to be addressed before the actual tritium Q value measurement can commence. The biggest is the ability to transfer ions from the external ion source to the Penning traps and also between the two Penning traps. Challenges are also expected with establishing an axial frequency lock with singly charged ^{3}He or ^{3}H ions. The axial linewidth for a given mass-to-charge ratio scales linearly with charge, and thus, the axial linewidth for singly charged ions is four times smaller than for the $^{12}C^{4+}$ ion. One way to address this problem is to increase the quality factor of the detection circuit by a factor of four. Also, instead of using mainly C_4 coupling, the cyclotron and axial modes can be coupled through the B_2 term. This works for any ion, regardless of its axial linewidth [1].

Additionally, the axial amplitude that is currently needed for detection is bigger than the thermal limit by a factor of ten, which has to be addressed by modifying the detection circuit. The occasionally appearing high drift rates of a few 10 ppt/h are also an issue, although by rapidly exchanging the ions of interest, this problem can be mitigated. It is worth noting that ^{3}H and ^{3}He form a mass doublet. Most notably, the amplitude-dependent systematic shifts are common for both and become negligible in their frequency ratio.

References

1. R.S. Van Dyck, Jr., D. B. Pinegar, S. Van Liew, S.L. Zafonte, Int. J. Mass Spectrom. **251**, 231 (2006)
2. Angrik, J., et al., Technical report, Karlsruher Institut für Technologie (KIT) (unpublished)
3. V. Aseev, et al., Phys. At. Nucl. **75**, 464 (2012)
4. C. Kraus, et al., Eur. Phys. J. C **40**, 447 (2005)
5. E.W. Otten, C. Weinheimer, Rep. Prog. Phys. **71**, 086201 (2008)
6. S.A. Thomas, F.B. Abdalla, O. Lahav, Phys. Rev. Lett. **105**, 031301 (2010)
7. S. Riemer-Sørensen, et al., Phys. Rev. D **85**, 081101 (2012)
8. H.V. Klapdor-Kleingrothaus, I.V. Krivosheina, A. Dietz, O. Chkvorets, Phys. Lett. B **586**, 198 (2004)
9. M. Agostini, et al., Phys. Rev. Lett. **111**, 122503 (2013)
10. S. Eliseev, T. Eronen, Yu. Novikov, Int. J. Mass Spectrom. **349–350**, 102 (2013)
11. E. Otten, J. Bonn, C. Weinheimer, Int. J. Mass Spectrom. **251**, 173 (2006)
12. M. Zbořil, et al., J. Instrum. **8**, P03009 (2013)
13. S. Rainville, J.K. Thompson, D.E. Pritchard, Science **303**, 334 (2004)
14. E.G. Myers, Int. J. Mass Spectrom. **349–350**, 107 (2013)
15. Sz. Nagy, et al., Europhys. Lett. **74**, 404 (2006)
16. G. Gräff, H. Kalinowsky, J. Traut, Zeitschrift für Physik A Atoms and Nuclei **297**, 35 (1980)
17. M. König, et al., Int. J. Mass Spectrom. Ion Processes **142**, 95 (1995)
18. M.L.E. Oliphant, P. Harteck, L. Rutherford, Proc. R. Soc. Lond. Ser. A **144**, 692 (1934)
19. G.C. Hanna, B. Pontecorvo, Phys. Rev. **75**, 983 (1949)
20. L.G. Smith, A.H. Wapstra, Phys. Rev. C **11**, 1392 (1975)
21. R.S. Van Dyck, Jr., D.L. Farnham, P.B. Schwinberg, Phys. Rev. Lett. **70**, 2888 (1993)
22. D.B. Pinegar, Ph.D. thesis, University of Washington, 2007
23. D.B. Pinegar, S.L. Zafonte, R.S. Van Dyck, Jr., Hyperfine Interact. **174**, 47 (2007)
24. C. Diehl, et al., Hyperfine Interact. **199**, 291 (2011)
25. R.S. Van Dyck, Jr., et al., Phys. Rev. Lett. **92**, 220802 (2004)
26. L.S. Brown, G. Gabrielse, Phys. Rev. A **25**, 2423 (1982)
27. J. Repp, et al., Appl. Phys. B **107**, 983 (2012)
28. C. Roux, et al., Appl. Phys. B **107**, 997 (2012)
29. D.B. Pinegar, et al., Rev. Sci. Instrum. **80**, 064701 (2009)
30. Ch. Böhm, et al., to be published
31. R.S. Van Dyck, Jr., D.L. Farnham, S.L. Zafonte, P.B. Schwinberg, Rev. Sci. Instrum. **70**, 1665 (1999)
32. G. Gabrielse, J. Tan, J. Appl. Phys. **63**, 5143 (1988)
33. R.S. Van Dyck, Jr., F.L. Moore, D.L. Farnham, P.B. Schwinberg, Phys. Rev. A **40**, 6308 (1989)
34. C. Diehl, Ph.D. thesis, Ruperto-Carola-University of Heidelberg, Germany, 2011
35. L.S. Brown, G. Gabrielse, Rev. Mod. Phys. **58**, 233 (1986)
36. F.L. Moore, et al., Phys. Rev. A **46**, 2653 (1992)
37. W.M. Haynes, (ed.) Ionization energies of atoms and atomic ions. *CRC Handbook of Chemistry and Physics*, 93rd edn, (Internet Version 2013), (CRC Press/Taylor and Francis, Boca Raton, 2013)